Polariton excitation in epsilon-near-zero slabs: Transient trapping of slow light

Alessandro Ciattoni,[1] Andrea Marini,[2] Carlo Rizza,[1,3] Michael Scalora,[4] and Fabio Biancalana[2,5]
[1]*Consiglio Nazionale delle Ricerche, CNR-SPIN, I-67100 L'Aquila, Italy*
[2]*Max Planck Institute for the Science of Light, Guenther-Scharowsky-Straße 1, D-91058 Erlangen, Germany*
[3]*Dipartimento di Scienza e Alta Tecnologia, Università dell'Insubria, via Valleggio 11, I-22100 Como, Italy*
[4]*Charles M. Bowden Research Center RDMR-WDS-WO, RDECOM, Redstone Arsenal, Alabama 35898-5000, USA*
[5]*School of Engineering & Physical Sciences, Heriot-Watt University, Edinburgh, EH14 4AS, United Kingdom*
(Received 22 March 2013; published 31 May 2013)

We numerically investigate the propagation of a spatially localized and quasimonochromatic electromagnetic pulse through a slab with a Lorentz dielectric response in the epsilon-near-zero regime, where the real part of the permittivity vanishes at the pulse carrier frequency. We show that the pulse is able to excite a set of virtual polariton modes supported by the slab, with the excitation undergoing a generally slow damping due to absorption and radiation leakage. Our numerical and analytical approaches indicate that in its transient dynamics the electromagnetic field displays the very same enhancement of the field component perpendicular to the slab, as in the monochromatic regime. The transient trapping is inherently accompanied by a significantly reduced group velocity ensuing from the small dielectric permittivity, thus providing an alternative platform for achieving control and manipulation of slow light.

DOI: 10.1103/PhysRevA.87.053853 PACS number(s): 42.25.Bs, 71.36.+c, 71.45.Gm

I. INTRODUCTION

Physical mechanisms driving to slow and fast light have attracted considerable attention from the scientific community in the past decade [1–3]. The inherent interest in slow light comes from the long matter-radiation interaction time, which can lead to considerable enhancement of all nonlinear processes that in turn may be exploited for active functionalities [4], e.g., all-optical switching and modulation [5,6]. The nonlinearity may also be enhanced by reducing the effective area in subwavelength silicon on insulator and plasmonic waveguides [7,8], where tight confinement opens up possibilities for miniaturized nonlinear applications [9–11]. Alternatively, extreme nonlinear dynamics [12,13], and enhanced second and third harmonic generation [14,15] is predicted in epsilon-near-zero (ENZ) metamaterials, where the linear susceptibility is tailored in such a way that its modulus becomes comparable to the nonlinear counterpart. Boosting the nonlinearity of ENZ plasmonic channels can also lead to active control of tunneling [16], switching, and bistable response [17]. ENZ metamaterials have also been used for directive emission [18,19], cloaking [20], energy squeezing in narrow channels [21], subwavelength imaging [22,23], and for investigating Anderson localization [24].

In all of the above-mentioned mechanisms, the trade-off needed to achieve enhanced active functionalities is paid in terms of increased losses. As a result, the ENZ regime one usually invokes refers to the case where the real part of the susceptibility becomes very small, while its imaginary part remains finite. Indeed, due to the stringent physical requirement of causality, Kramers-Kronig relations impose that dispersion be inherently accompanied by loss and the dielectric susceptibility cannot become rigorously null [25]. The residual loss either limits or even prevents giant enhancement of coherent mechanisms, e.g., in second and third harmonic generation setups [14,15]. Recently, in the context of surface plasmon polaritons, a method has been proposed to overcome the loss barrier for superlensing applications by loading the effect of loss into the time domain [26]. In our analytical calculations, we will use a similar approach to study the behavior of an electromagnetic pulse that scatters from a slab having a Lorentz dielectric response. Indeed, by considering nonmonochromatic *virtual modes* with complex frequency [27], it is possible to drop off the effect of loss on the temporal dependence of the "mode" itself. In this complex frequency approach, it is possible to achieve the condition where the dielectric susceptibility exactly vanishes. Our formalism treats the dielectric polarization of the medium as a generic Lorentz oscillator that, in the epsilon-equal-to-zero condition, encompasses longitudinal collective oscillations of both electrons (volume plasmons) and ions (longitudinal phonons) that cannot be excited by light [28]. Recently, the question as to whether or not volume plasmons can be excited by classical light has been revived [29–33]. Some studies on Mie extinction efficiencies reveal a maximum around the characteristic frequency where the dielectric susceptibility vanishes, attributing the enhanced extinction to the excitation of volume plasmons [30,32]. Conversely, other similar studies identify the physical origin of the enhanced extinction in the excitation of leaky modes [29,31]. The latter interpretation is also supported by studies of the excitation of surface phonon polaritons in ENZ slabs [34–37].

In this paper we numerically investigate and analytically interpret the scattering of a spatially and temporally localized optical pulse from a dielectric slab in the ENZ regime. We used a finite-difference time-domain (FDTD) algorithm to solve the full vectorial Maxwell equations coupled to the Lorentz oscillator equation for the dielectric polarization of the slab. We find that, if the carrier frequency of the optical pulse matches the ENZ condition, electromagnetic quasitrapping occurs within the Lorentz slab since, after the pulse has passed through it, an elecromagnetic-polarization (polariton) oscillation persists and generally slowly damps out. We demonstrate that nontrivial ENZ features such as the enhancement of the longitudinal electric field component are still observable in the time domain. We also find that

the above-mentioned phenomenon is not observed for optical pulses with carrier frequencies far from the ENZ condition. Thus, in order to grasp the underpinning physical mechanisms responsible for transient trapping in the ENZ regime, we analytically investigate the scattering features of the Lorentz slab by studying the virtual leaky modes of the structure. We recognize that a set of polariton modes with reduced transverse group velocity ($v_g \simeq c/100$, where c is the speed of light in vacuum) is excited. Indeed, the plasma frequency plays the role of a cutoff frequency and polaritons in the ENZ regime are intrinsically characterized by a reduced group velocity. Thus, we are able to interpret the transient trapping by means of the excitation of slow polariton modes that are damped off due to medium absorption and radiation leakage in the outer medium.

The paper is organized as follows. In Sec. II we report the results of numerical finite-difference time-domain (FDTD) simulations, comparing the distinct phenomenologies occurring in ENZ and standard dielectric regimes. In Sec. III we analytically investigate the virtual leaky modes of the structure, we address their properties, and we discuss their role in the interpretation of numerical results just developed in Sec. III. In Sec. IV we draw our conclusions.

II. FINITE-DIFFERENCE TIME-DOMAIN ANALYSIS OF THE TIME-DOMAIN ENZ REGIME

A. Pulse scattering by a Lorentz slab

Let us consider the scattering interaction illustrated in Fig. 1(a), where an electromagnetic pulse is launched along the z axis in vacuum and orthogonally impinges on the surface of a dielectric slab. The pulse is a transverse magnetic (TM) excitation, with electric $E_x(x,z,t)$, $E_z(x,z,t)$ and magnetic $H_y(x,z,t)$ field components. As it is well known, the time evolution of the TM pulse forward propagating along the z axis can be evaluated if one of the three field components is known at a single plane (say, $z = z_{\rm in}$ for the input plane) at any time t. Therefore, for $E_x^{(+)}$, the forward propagating component of E_x, we set

$$E_x^{(+)}(x,z_{\rm in},t) = E_0 e^{-\frac{x^2}{w_x^2}} e^{-\frac{(t-t_0)^2}{\tau^2}} \sin(\bar{\omega}t), \tag{1}$$

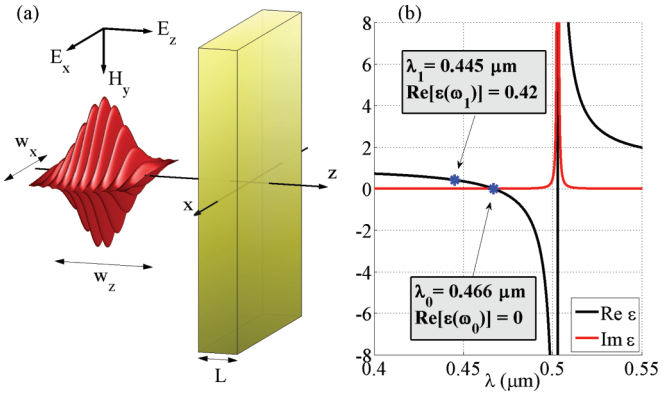

FIG. 1. (Color online) (a) Interaction geometry of the pulse colliding onto the dielectric slab. (b) Real and imaginary parts of the slab dielectric permittivity for the Lorentz parameters used in the FDTD analysis as a function of the wavelength.

which is both spatially (along the x axis) and temporally localized, w_x and τ being its transverse and temporal widths, respectively. As a consequence of the temporal profile at $z = z_{\rm in}$, the pulse, during propagating along the z axis, will have a longitudinal width $w_z \simeq c\tau$ [see Fig. 1(a)]. The pulse is temporally localized at the time t_0 and it is modulated by a carrier with frequency $\bar{\omega}$. As a consequence, $\bar{\omega}$ is the pulse central frequency and $\delta\omega \simeq 1/\tau$ is the spectral width. Hereafter we will focus on quasimonochromatic pulses for which the condition $\delta\omega/\bar{\omega} \ll 1$ is satisfied.

The dielectric slab has width L, it is centered at $(x,z) = (0,0)$, and we assume that, in the presence of the external electric field $\mathbf{E}$, the dynamics of its dielectric polarization is governed by the Lorentz oscillator model

$$\frac{d^2\mathbf{P}}{dt^2} + \gamma\frac{d\mathbf{P}}{dt} + \omega_e^2\mathbf{P} = \epsilon_0 f_e \mathbf{E}, \tag{2}$$

where ω_e is the resonant angular frequency, γ is the damping constant, f_e is the oscillator strength, and ϵ_0 is the dielectric permittivity of vacuum. It is well known that Eq. (2) leads, in the frequency domain, to the constitutive relation $\tilde{\mathbf{D}}_\omega = \epsilon_0\epsilon(\omega)\tilde{\mathbf{E}}_\omega$, where $\tilde{f}_\omega = \int_{-\infty}^{+\infty} dt e^{i\omega t} f(t)$ is the Fourier transform of $f(t)$, $\mathbf{D} = \epsilon_0\mathbf{E} + \mathbf{P}$ is the displacement field vector, and

$$\epsilon(\omega) = 1 + \frac{f_e}{\omega_e^2 - i\gamma\omega - \omega^2} \tag{3}$$

is the frequency-dependent medium dielectric permittivity. By performing the inverse Fourier transform of the relation $\tilde{\mathbf{D}}_\omega = \epsilon_0\epsilon(\omega)\tilde{\mathbf{E}}_\omega$, one easily obtains the well-known result

$$\begin{aligned} \mathbf{D(t)} &= \epsilon_0\left[\mathbf{E}(t) + \int_{-\infty}^{t} dt'\chi(t-t')\mathbf{E}(t')\right], \\ \chi(T) &= f_e e^{-\frac{\gamma T}{2}} \frac{\sin\left(\sqrt{\omega_e^2 - \frac{\gamma^2}{4}}\,T\right)}{\sqrt{\omega_e^2 - \frac{\gamma^2}{4}}}, \end{aligned} \tag{4}$$

where $\chi(T)$ is the time-dependent Lorentz susceptibility. The realistic model of Eq. (2) is particularly accurate for describing the medium dielectric response to fields with frequencies close to the resonant frequency ω_e (so that contributions due to other resonances can be neglected). Therefore, the Lorentz model is particularly suitable for our analysis since we are here concerned with quasimonochromatic pulses whose carrier frequency $\bar{\omega}$ coincides with (or is close to) the frequency

$$\omega_0 = \sqrt{\frac{1}{2}\left[\left(2\omega_e^2 - \gamma^2 + f_e\right) + \sqrt{f_e^2 + \gamma^2\left(\gamma^2 - 4\omega_e^2 - 2f_e\right)}\right]}, \tag{5}$$

where the real part of the permittivity vanishes, i.e., $\mathrm{Re}\,[\epsilon(\omega_0)] = 0$, the so-called epsilon-near-zero (ENZ) regime.

We have performed the numerical analysis of the pulse-slab collision by means of a finite-difference time-domain (FDTD) scheme where the polarization dynamics of Eq. (2) are coupled to Maxwell equations for the TM field. Specifically, in order to isolate the relevant phenomenon characterizing the ENZ regime, we have analyzed through FDTD simulations two

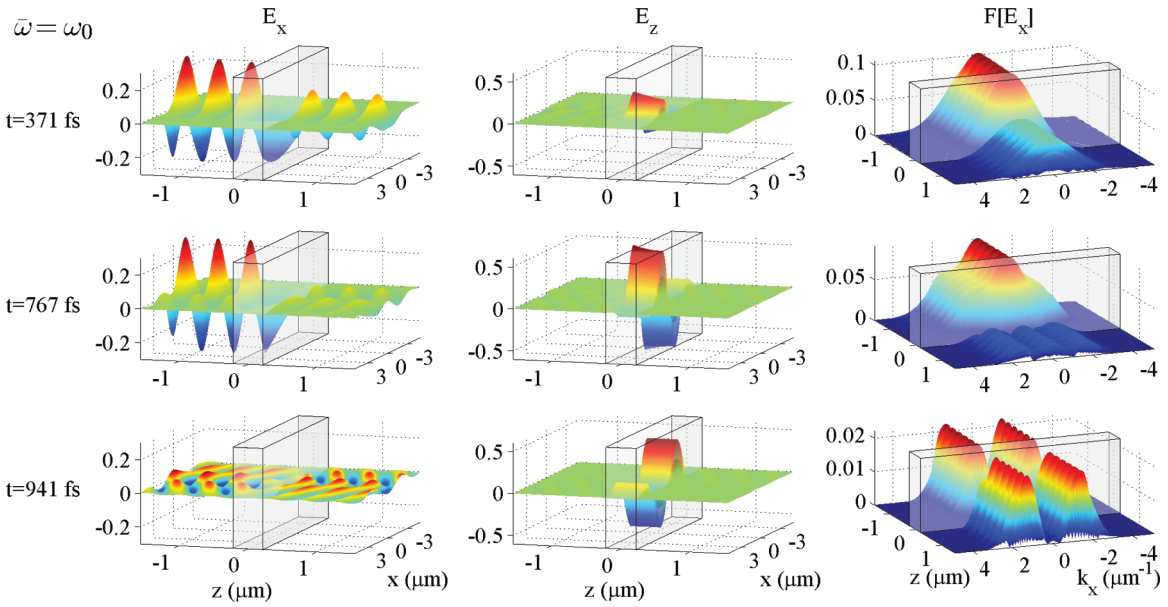

FIG. 2. (Color online) Results of the FDTD simulation pertaining to the interaction of pulse 0 (with $\bar{\omega} = \omega_0$) with the slab. The fields E_x,E_z and the Fourier transform $F[E_x]$ are captured at three different time steps corresponding to the three rows. In the first and the second time steps the pulse peak is just behind and beyond the slab, respectively, whereas in the third time step the pulse has completely left the slab. Note the large E_z component within the slab (signature of the epsilon-near-zero regime) and the persisting and pulse-free polariton oscillation in the third time step. Arbitrary units are used for the field components.

different situations where the same dielectric slab is hit by two spatially equal pulses with different carrier frequencies $\bar{\omega}$: The first (pulse 0) is such that $\bar{\omega} = \omega_0$ so that it is suitable to scan the slab behavior in its ENZ regime; the second (pulse 1) has $\bar{\omega} = \omega_1$ for which $\mathrm{Re}[\epsilon(\omega_1)] > 0$ so that it experiences standard dielectric behavior.

In view of the generality and ubiquity of the Lorentz model of Eq. (2), we have chosen for our numerical simulations a medium with Lorentz parameters $\omega_e = 3.75 \times 10^{15}$ Hz, $\gamma = 1.50 \times 10^{12}$ s^{-1}, and $f_e = 2.25 \times 10^{30}$ s^{-2}. These parameters have been chosen in order to deal with optical pulses in the visible spectrum, the resonant frequency corresponding to the wavelength $\lambda_e = 2\pi c/\omega_e = 0.502$ μm (evidently, different values of the Lorentz model would give analogous results at different frequencies for appropriate slabs of scaled thickness). For such parameters Eq. (5) yields $\omega_0 = 4.03 \times 10^{15}$ Hz and we have set $\omega_1 = 4.23 \times 10^{15}$ Hz (for which $\mathrm{Re}[\epsilon(\omega_1)] = 0.42$), the two frequencies corresponding to the wavelengths $\lambda_0 = 2\pi c/\omega_0 = 0.466$ μm and $\lambda_1 = 2\pi c/\omega_1 = 0.445$ μm, respectively. In Fig. 1(b) we plot the real and imaginary parts of the dielectric permittivity for the chosen Lorentz parameters as functions of the wavelength $\lambda = 2\pi c/\omega$, indicating the carrier wavelengths λ_0 and λ_1 that characterize the two pulses. We have set $t_0 = 500$ fs and we have chosen a slab width $L = 0.41$ μm to minimize the pulse propagation features and to effectively highlight the impact of the medium polarization on field dynamics. For the pulse spatial and temporal widths we have chosen $w_x = 1$ μm and $\tau = 200$ fs: The former is comparable to the central wavelength of the pulse for providing it a non-negligible longitudinal field component E_z (see below) whereas the latter corresponds to a spectral width $\delta\omega \simeq 1/\tau = 5 \times 10^{12}$ Hz so that the pulses are in the quasimonochromatic regime.

B. Pulse 0 scattering

In Fig. 2 we report the main results of the FDTD simulation dealing with the interaction of pulse 0 with carrier frequency $\bar{\omega} = \omega_0$ with the Lorentz slab represented in the figure by semitransparent rectangular blocks. The first two columns of the figure contain the plots of $E_x(x,z,t)$, $E_z(x,z,t)$ as functions of (x,z) whereas the third contains the Fourier transform $F[E_x](k_x,z,t) = \int_{-\infty}^{+\infty} dx e^{ik_x x} E_x(x,z,t)$ as a function of (k_x,z); each row of the figure corresponds to a selected simulation time step. At the first time step (first row of Fig. 2), $t = 371$ fs, the pulse is fully interacting with the slab (the pulse peak being about to hit the slab at $t = 500$ fs) and the electromagnetic field is characterized by standard reflection and transmission features; in particular, both the reflected and transmitted pulses have a transverse bell-shaped spatial profile and accordingly the Fourier transform $F[E_x]$ is peaked as well. Note however that, even in this early transient stage of the interaction, within the slab the longitudinal component E_z is comparable to E_x and is much greater than its vacuum counterpart. Such an enhancement of the electric field component perpendicular to the slab is a feature typically associated with the *monochromatic* ENZ regime, arising as a consequence of the continuity of the displacement field component perpendicular to the interface [14,15]. Therefore this is evidence that the ENZ regime can effectively be observed in thoroughly realistic Lorentz slabs by means of an equally realistic scattering interaction configuration. The second row of Fig. 2 corresponds to the time step $t = 767$ fs, a time when the incoming pulse (if freely propagating) would have passed behind the slab (its temporal width being 200 fs). Note that the longitudinal component E_z is even greater than the previous time step, testifying to the fact that the ENZ regime also occurs in the time domain. The transverse

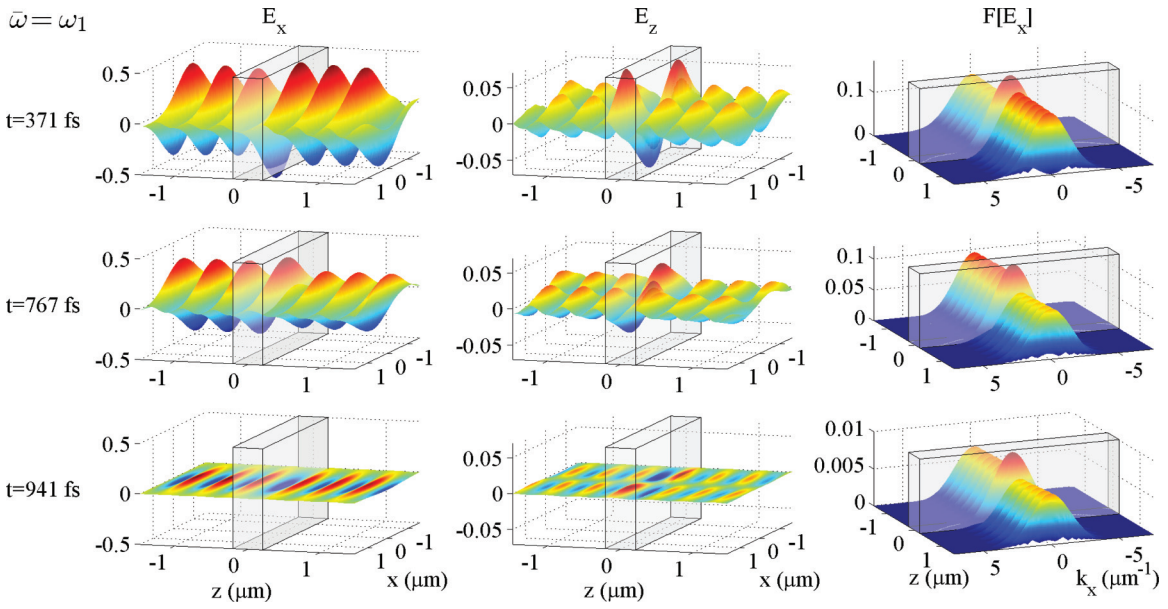

FIG. 3. (Color online) Results of the FDTD simulation pertaining to the interaction of pulse 1 (with $\bar{\omega} = \omega_1$) with the slab. The fields E_x,E_z and the Fourier transform $F[E_x]$, for comparison purposes, are captured at same time steps considered in Fig. 2. Note that both E_x and $F[E_x]$ are bell shaped, that magnitudes of E_z within the slab and in vacuum are comparable, and that no residual polariton oscillation has been produced by pulse passage. Arbitrary units are used for the field components.

component E_x shows different spatial features, even more evidently displayed by its Fourier transform $F[E_x]$ which is no longer bell shaped and is characterized by a complex multistructured profile. The third row of Fig. 2 considers a later time step $t = 941$ fs that is much longer than the time spent by the pulse to fully travel into the slab and leave it. At this time step, the longitudinal component E_z is *still* very large within the slab and the transverse component E_x displays different and unexpected features: It is symmetric under the reflection $z \to -z$, it is not transversally bell shaped, and its Fourier transform $F[E_x]$ displays two peaks at the sides of $k_x = 0$. Such phenomena can be interpreted only by assuming that the interaction of pulse 0 with the slab is accompanied by the excitation of a polariton mode whose oscillation lasts a time much longer than the pulse-slab interaction time.

C. Pulse 1 scattering

In order to appreciate the above-discussed time-domain ENZ phenomena, we now discuss the interaction of pulse 1 with the slab, its carrier frequency being associated with *standard* slab dielectric behavior. In Fig. 3 we report the results of the FDTD simulation relative to pulse 1 and, for comparison purposes, we have given Fig. 3 the same structure as Fig. 2 with the same fields at the same time steps. Remarkably, both E_x and $F[E_x]$ are everywhere and always bell shaped, while the magnitude of E_z within the slab is comparable to its vacuum magnitude. At the last time step the slab hosts no residual polariton oscillation resulting from the pulse passage. This is precisely the standard expected phenomenon of the reflection and transmission of the pulse by a dielectric slab, and the comparison with the results of Fig. 2 proves that the phenomenon it contains is a manifestation of the time-domain ENZ regime.

D. Transient trapping in the time-domain epsilon-near-zero regime

In addition to the remarkable fact that the same features of the monochromatic ENZ regime characterize its time-domain counterpart (e.g., the slab hosts a pronounced enhancement of the field E_z), the results discussed in the previous sections also clearly reveal that the scattering situation leads to the unique excitation of a polariton mode. In order to show more explicitly such a phenomenon, in Fig. 4 we have plotted the fields E_x and E_z, for both pulse 0 and pulse 1 as functions of (z,t) at a fixed plane $x = x_p = 1.76$ μm. The evident feature that emerges is that pulse 0 [see Figs. 4(a) and 4(b)] produces a strong and damped electromagnetic self-oscillation persisting for a time (about 5500 fs) that is much longer than the probing pulse duration (200 fs), self-oscillation which is conversely not produced by pulse 1 [see Figs. 4(c) and 4(d)], and whose electromagnetic track fades within the slab just after it has left the medium (at about $t = 1000$ fs). We conclude that, in the ENZ regime, the pulse traveling through the slab triggers an alternative mechanism of transient light trapping. The same phenomenon is also reported in Fig. 5, where the input [at $(x,z,t) = (0, -L/2,t)$] and the output [at $(x,z,t) = (0,L/2,t)$] E_x components of pulse 0 [Fig. 5(a)] and pulse 1 [Fig. 5(b)] are reported together with their temporal Fourier transform. The profile of the output field for pulse 1 clearly shows the outgoing pulse followed by a damped oscillation associated with the transient light trapping. Accordingly, the corresponding temporal spectrum is a replica of the incoming pulse spectrum with a central hole associated with the excitation of internal slab modes supporting the radiation trapping. As far as pulse 1 is concerned [Fig. 5(b)], no light trapping occurs and the spectrum of the outgoing pulse does not show the hole appearing in Fig. 5(a).

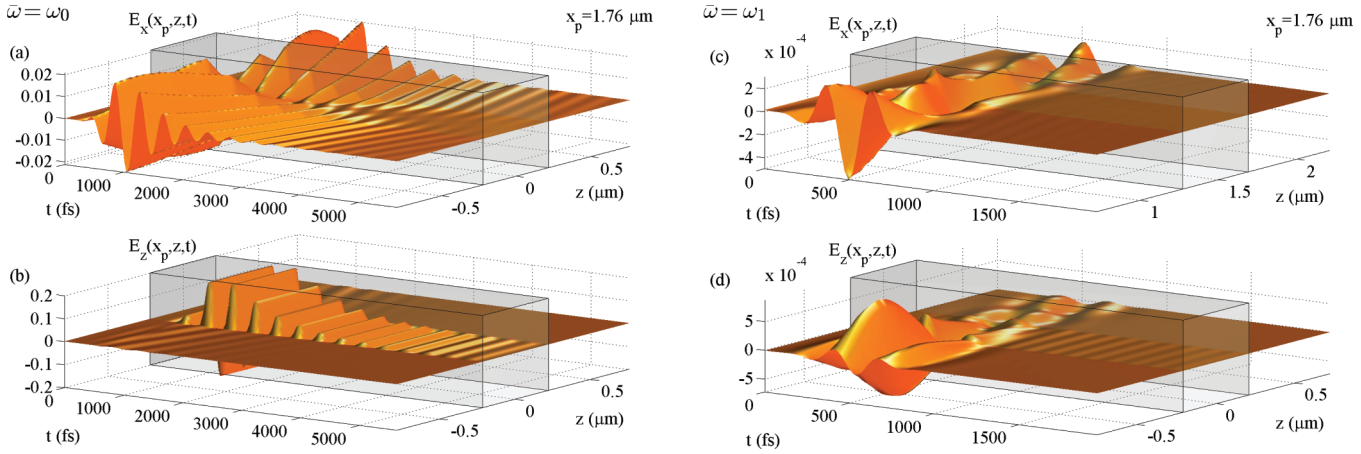

FIG. 4. (Color online) FDTD predictions about the fields E_x and E_z, for both pulse 0 and pulse 1 as function of (z,t) at a fixed plane $x = x_p = 1.76\ \mu$m. Pulse 0 triggers an alternative mechanism of metastable light trapping since its passage produces a strong and damped polariton oscillation which is absent in the case of pulse 1. Arbitrary units are used for the field components.

III. THEORETICAL ANALYSIS OF TIME-DOMAIN ENZ REGIME

A. Polariton virtual mode analysis

From the above-discussed phenomenon, it is evident that a quasimonochromatic pulse with a spectrum centered at the zero of the real part of the slab permittivity excites a polariton mode that lasts for a time much longer than the pulse-slab interaction time. In order to rigorously prove this statement and gain a deeper understanding of the underpinning physical mechanisms that support the time-domain ENZ regime, in this section we analyze the exact quasisteady modes (virtual modes) of the slab. In our analysis we fully take into account damping processes, which include medium absorption and radiation leakage in vacuum, adopting the complex frequency approach [27]. We start our analysis from the curl Maxwell equations for TM fields,

$$\begin{aligned} -\frac{\partial E_z}{\partial x} + \frac{\partial E_x}{\partial z} &= -\mu_0 \frac{\partial H_y}{\partial t}, \\ -\frac{\partial H_y}{\partial z} &= \epsilon_0 \frac{\partial E_x}{\partial t} + \frac{\partial P_x}{\partial t}, \\ \frac{\partial H_y}{\partial x} &= \epsilon_0 \frac{\partial E_z}{\partial t} + \frac{\partial P_z}{\partial t}, \end{aligned} \tag{6}$$

where the polarization $\mathbf{P}(x,z,t) = P_x(x,z,t)\hat{\mathbf{e}}_x + P_z(x,z,t)\hat{\mathbf{e}}_z$ satisfies Eq. (2) within the slab ($|z| < L/2$) and it vanishes outside the slab ($|z| > L/2$). We take the ansatz $A_j(x,z,t) = \mathrm{Re}[a_j(z)e^{i(k_x x - \Omega t)}]$ for every field component ($A = E,H,P$, $a = e,h,p$, and $j = x,z$), where k_x is the (real) transverse wave vector and $\Omega = \omega - i\Gamma$ is the complex angular frequency with $\Gamma > 0$ so that only damping modes are considered. Owing to the mutual temporal evolution of the electromagnetic field $(\mathbf{E},\mathbf{H})$ and of the polarization field $\mathbf{P}$, the ansatz effectively amounts to considering polariton virtual modes. The magnetic field can be expressed in terms of the electric field components $h_y = -(k_x e_z + i\partial_z e_x)/(\mu_0\Omega)$ so that Maxwell's equations reduce to

$$e_z = \frac{ik_x}{\frac{\Omega^2}{c^2}\tilde{\epsilon}(\Omega,z) - k_x^2}\frac{de_x}{dz}, \tag{7}$$

$$\frac{d^2 e_x}{dz^2} + \left[\frac{\Omega^2}{c^2}\tilde{\epsilon}(\Omega,z) - k_x^2\right]e_x = 0, \tag{8}$$

where $\tilde{\epsilon}(\Omega,z) = \epsilon(\Omega)\theta(L/2 - |z|) + \theta(|z| - L/2)$ [$\theta(z)$ being the Heaviside step function] is the z-dependent dielectric profile. It is worth stressing that the permittivity ϵ is evaluated at the complex frequency Ω. The general solution of Eqs. (7)

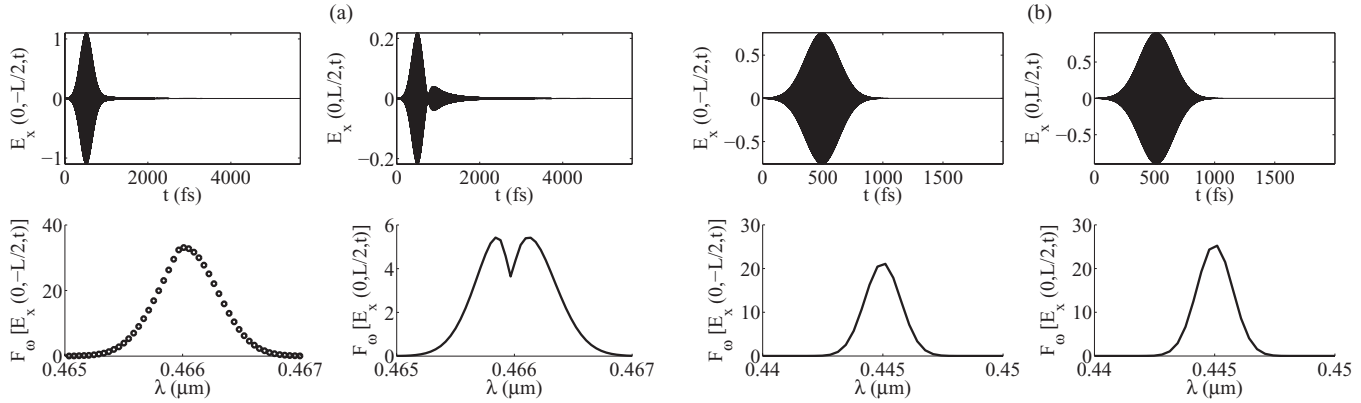

FIG. 5. Electric field x component E_x of (a) pulse 0 and (b) pulse 1 evaluated at $(x,z,t) = (0,-L/2,t)$ and $(x,z,t) = (0,L/2,t)$, together with their temporal Fourier transform $F_\omega[E_x]$. Arbitrary units are used for the field components.

and (8) is explicitly given by

$$e_x(z) = C \begin{cases} \Theta e^{-i\Xi K\left(z+\frac{L}{2}\right)}, & z < -\frac{L}{2}, \\ \frac{e^{ikz}+\Theta e^{-ikz}}{e^{ik\frac{L}{2}}+\Theta e^{-ik\frac{L}{2}}}, & -\frac{L}{2} \leqslant z \leqslant \frac{L}{2}, \\ e^{i\Xi K(z-L/2)}, & z > \frac{L}{2}, \end{cases} \tag{9}$$

$$e_z(z) = C \begin{cases} \Theta\Xi\frac{k_x}{K} e^{-i\Xi K\left(z+\frac{L}{2}\right)}, & z < -\frac{L}{2}, \\ \frac{k_x}{k}\frac{-e^{ikz}+\Theta e^{-ikz}}{e^{ik\frac{L}{2}}+\Theta e^{-ik\frac{L}{2}}}, & -\frac{L}{2} \leqslant z \leqslant \frac{L}{2}, \\ -\Xi\frac{k_x}{K} e^{i\Xi K\left(z-\frac{L}{2}\right)}, & z > \frac{L}{2}, \end{cases}$$

where $K = \sqrt{\frac{\Omega^2}{c^2} - k_x^2}$, $k = \sqrt{\frac{\Omega^2}{c^2}\epsilon(\Omega) - k_x^2}$, C is the arbitrary mode amplitude, $\Theta = \pm 1$ is a parameter that distinguishes the symmetry of the solutions, and $\Xi = \pm 1$ is another parameter selecting the sign of the exponentials in vacuum. By construction, the modal fields in Eqs. (9) already satisfy the continuity of the field component parallel to the slab surface (e_x) at the interfaces $x = \pm L/2$. The boundary conditions (BCs) for the continuity of the displacement field component ($\tilde{\epsilon} e_z$) perpendicular to the interfaces $x = \pm L/2$ yield the dispersion relation

$$(K\epsilon - \Xi k)\, e^{ikL} = \Theta(K\epsilon + \Xi k), \tag{10}$$

which provides the complex frequency Ω for every given slab thickness L and transverse wave vector k_x. We have solved Eq. (10) numerically and obtained the allowed Ω corresponding to different values of k_x using the same slab thickness and Lorentz dispersive parameters of the slab considered in Sec. II. In Fig. 6 we plot the results for the case $\Theta = -1$ in the complex plane Ω parametrized through the wavelength λ and the damping constant Γ (i.e., $\Omega = 2\pi c/\lambda - i\Gamma$), using circles and stars for the $\Xi = -1$ and $\Xi = 1$ modes, respectively, and using the marker color to label the value of the corresponding k_x. Note that the $\Xi = -1$ and $\Xi = 1$ modes belong to two different branches which are characterized by the fact that the $\Xi = -1$ modes have a damping constant that is greater than the $\Xi = +1$ modes. This property can be easily understood by considering the z component of the nonoscillatory part of the

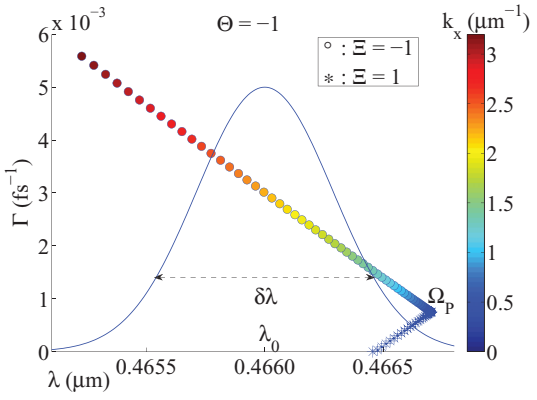

FIG. 6. (Color online) Virtual modes of the slab considered in Sec. II for the symmetry $\Theta = -1$ in the complex plane $\Omega = 2\pi c/\lambda - i\Gamma$. Circles and stars label the $\Xi = -1$ and $\Xi = 1$ modes whereas the marker color labels the corresponding k_x value. The complex frequency Ω_P is such that $\epsilon(\Omega_P) = 0$. The thin continuous line is the temporal spectrum of the incoming pulse reported in arbitrary units.

Poynting vector $\mathbf{S} = \mathbf{E} \times \mathbf{H}$ for $z > L/2$:

$$\langle S_z \rangle = \Xi e^{-2[\Xi\,\mathrm{Im}(K)(z-\frac{L}{2})+\Gamma t]} \frac{1}{2}\epsilon_0\,\mathrm{Re}\left(\frac{\Omega}{K}\right)|C|^2. \tag{11}$$

For $\Xi = -1$, the energy outflows from the slab and the damping of the virtual mode is more rapid since it loses energy through both medium absorption and radiation leakage. Conversely, for $\Xi = 1$ the electromagnetic energy is dragged into the slab, thus partially compensating for the medium absorption and consequently decreasing the virtual mode damping time (note that there is also a point where $\Gamma = 0$ on the $\Xi = 1$ branch corresponding to the exact balance between medium absorption and radiation drag). It is remarkable that the $\Xi = -1$ and $\Xi = 1$ branches intersect each other at point Ω_P for $k_x \to 0$. In this limit the dispersion relation of Eq. (10) (for $\Theta = -1$) reduces to

$$e^{i\frac{\Omega_P}{c}\sqrt{\epsilon(\Omega_P)}} = \frac{\Xi - \sqrt{\epsilon(\Omega_P)}}{\Xi + \sqrt{\epsilon(\Omega_P)}}, \tag{12}$$

and is satisfied only if $\epsilon(\Omega_P) = 0$. Starting from the Lorentz model, it is straightforward to prove that the permittivity vanishes at $\Omega_P = \sqrt{f_e + \omega_e^2 - \gamma^2/4 - i\gamma/2}$ that, for the above-used Lorentz dispersive parameters, yields $\lambda_P = 2\pi c/\mathrm{Re}(\Omega_P) = 0.4667\ \mu\mathrm{m}$ and $\Gamma_P = -\mathrm{Im}(\Omega_P) = 8.3 \times 10^{-3}\ \mathrm{fs}^{-1}$, precisely matching the point of Fig. 6 where the two branches $\Xi = \pm 1$ intersect each other. In turn, the *plasmonic* Ω_P at which the permittivity vanishes plays a central role in the analysis of the virtual modes. For the complex frequencies Ω reported in Fig. 6, $|\epsilon(\Omega)| < 0.06$ and therefore all the obtained modes with symmetry $\Theta = -1$ imply the time-domain ENZ regime.

In the same portion of the complex plane Ω we have numerically found no allowed modes for the symmetry $\Theta = 1$. This can be grasped by expanding both sides of Eq. (10) in a Taylor series of ϵ (since $|\epsilon(\Omega)| \ll 1$); at the zeroth order we readily obtain $e^{-k_x L} = -\Theta$ which is not consistent if $\Theta = 1$ (and which, on the other hand, yields $k_x = 0$ for $\Theta = -1$).

B. Interpretation of FDTD results in terms of virtual polariton modes and slow-light regime

Usually, within the standard real frequency approach, the solutions for the slab modes with $\Xi = -1$ are disregarded since they are considered unphysical. Indeed, if $|k_x| > \omega/c$, the solutions with $\Xi = +1$ represent confined modes propagating along the x direction, while solutions with $\Xi = -1$ are unbound modes that diverge at $z \to \pm\infty$. In addition, the introduction of the complex frequency introduces an inherent field singularity in the past $t \to -\infty$. Due to such intrinsic singularities, it is strictly impossible to rigorously excite a single virtual mode, its global existence on the whole space-time being unphysical. However, both singularities occur asymptotically and therefore virtual modes provide a very adequate description of the transient ENZ slab behavior occurring within a spatially bounded region and through a finite-time lapse. In order to prove this statement and to basically provide a theoretical description of the transient light trapping discussed in Sec. II D, in Fig. 6 we have superimposed the temporal spectrum profile of the incoming pulse of Eq. (1) (using the thin continuous line) on the

complex-plane virtual modal structure. Note that, due to its wavelength bandwidth $\delta\lambda = (2\pi c/\omega_0^2)\delta\omega = 5.8 \times 10^{-4}\ \mu$m, the pulse spectrum centered at λ_0 overlaps a limited portion of the considered complex frequency plane so that, specifically, the sole virtual modes with $|\lambda - \lambda_0| < \delta\lambda/2$ are actually excited by the considered pulse 0. From Fig. 6 it is evident that the excited virtual modes are characterized by the transverse wave vector k_x spanning the range $1.1\ \mu\text{m}^{-1} < k_x < 2.7\ \mu\text{m}^{-1}$ and that, due to the finite bandwidth of the impinging pulse, the excited virtual modes with the largest amplitude are those around the central transverse wave vector $k_x = 1.9\ \mu$m, which corresponds to $\lambda = 2\pi c/\text{Re}(\Omega)$ close to $\lambda_0 = 0.466$. This observation is in striking agreement with the results contained in Fig. 2, where one can see that the transverse Fourier transform of the field has, at the latest time step, two peaks centered at $k_x \simeq 1.9\ \mu$m and $k_x \simeq -1.9\ \mu$m whose width is of the order of $\delta k_x \simeq 0.8\ \mu$m. Therefore, when pulse 0 impinges onto the slab, it excites precisely the virtual modes analytically predicted in Sec. III A, which are compatible to its spectral structure. As a further validation of this statement, note that the virtual modes excited by pulse 0 ($|\lambda - \lambda_0| < \delta\lambda/2$) have a damping constant Γ spanning the range $1.2 \times 10^{-3}\ \text{fs}^{-1} < \Gamma < 4.9 \times 10^{-3}\ \text{fs}^{-1}$ (see Fig. 6), which corresponds to the extinction time $\tau = 3/\Gamma$ spanning the range 609 fs $< \tau <$ 2604 fs. Also this prediction based on the above virtual mode analysis is in striking agreement with the FDTD results since, by looking at Figs. 4(a) and 4(b), one can see that the electromagnetic excitation persists for a time of the order of 3000 fs, which is compatible with the maximum extinction time of the excited virtual modes. In addition, the spatial symmetry of the $\Theta = -1$ virtual polariton modes matches the numerical results displayed in Fig. 4: The transverse field component (e_x) is antisymmetric with respect to the $z = 0$ axis, whereas the longitudinal field component (e_z) is symmetric.

The final ingredient needed to thoroughly interpret the transient light trapping observed in FDTD simulations is related to the intrinsic slow-light nature of the phenomenon, which may be preliminarily grasped by considering a bulk Lorentz medium, where transverse plane waves satisfy the dispersion relation $k(\omega) = (\omega/c)\sqrt{\epsilon(\omega)}$. Neglecting medium absorption ($\gamma \simeq 0$), one finds that the phase velocity is $v_f = \omega/k$ and the group velocity $v_g = d\omega/dk$ is

$$v_g(\omega) = c\left[\sqrt{\epsilon(\omega)} + \frac{f_e\omega^2}{\sqrt{\epsilon(\omega)}\left(\omega_e^2 - \omega^2\right)^2}\right]^{-1}. \qquad (13)$$

Thus, in the ENZ regime, the phase velocity diverges $v_f \to \infty$ whereas the group velocity tends to zero $v_g \to 0$. Even though the subwavelength Lorentz slab used in our FDTD simulations is not a bulk medium and absorption has not been neglected, the rough argument above still predicts the correct outcome. Indeed, by numerically solving the dispersion relation of Eq. (10) without neglecting losses, one finds that, at the optical wavelength λ_0, the transverse phase velocity of virtual polariton modes is superluminal, $v_f = \omega/k_x \simeq 10c$, while the transverse group velocity is extremely reduced, $v_g = d\omega/dk_x \simeq c/100$. For this reason, it is now clear how the virtual polariton modes, once excited, do not disperse quickly in the x direction and remain quasitrapped within the slab owing to the tremendously reduced temporal dynamics. We conclude that the above-described transient light trapping can be fully interpreted and physically understood by means of slow polariton modes supported by the slab.

C. Volume plasmons

Although the above-discussed numerical and analytical analysis of the transient light trapping characterizing the time-domain ENZ regime is quite exhaustive, we now discuss its connection with the purely longitudinal modes, either *volume plasmons* (collective oscillations of electrons) or *volume phonons* (collective oscillations of ions), which the Lorentz medium can support. Hereafter we focus on volume plasmons, considering an unbounded bulk Lorentz medium where the TM electromagnetic and polarization dynamics are described by Eqs. (2) and (6). For the plane-wave ansatz $A_j(x,z,t) = \text{Re}[a_j e^{i(k_x x + k_z z - \Omega t)}]$, where $A = E,H,P$, $a = e,h,p$, $j = x,z$, k_x,k_z are the (real) wave-vector components, and Ω is the generally complex frequency, one gets

$$\begin{aligned} \mu_0\Omega h_y &= -k_x e_z + k_z e_x, \\ k_z h_y &= \Omega\epsilon_0\epsilon(\Omega) e_x, \\ k_x h_y &= -\Omega\epsilon_0\epsilon(\Omega) e_z, \end{aligned} \qquad (14)$$

where $\epsilon(\Omega)$ is the dielectric permittivity with complex frequency Ω. Volume plasmons are purely longitudinal electric oscillations owing to the collective motion of electrons and are not accompanied by the generation of a magnetic field, a feature that for plane waves amounts to the collinearity of the wave vector $\mathbf{k} = k_x\hat{\mathbf{e}}_x + k_z\hat{\mathbf{e}}_z$ and the electric field $\mathbf{E} = k_x\hat{\mathbf{E}}_x + k_z\hat{\mathbf{E}}_z$. Therefore, imposing the condition $\mathbf{k} \times \mathbf{E} = 0$, i.e., $-k_x e_z + k_z e_x = 0$, Eqs. (14) readily yield $h_y = 0$ and $\epsilon(\Omega_P) = 0$. Thus, volume plasmons are inherently involved in the time-domain ENZ regime we are considering in this paper. However, it is worth noting that the virtual modes of the Lorentz slab are polaritons, entities fundamentally different from volume plasmons (or volume phonons). Indeed, a volume plasmon is strictly characterized by the condition $\epsilon(\Omega) = 0$ that implies the severe dispersion $\Omega = \Omega_P$ and, in the presence of the slab boundaries at $z = \pm L/2$, inevitably leads to the inconsistency $E_z \to \infty$ within the slab unless $E_z = 0$ in the outer medium. This is consistent with the well-known *impossibility* to excite volume plasmons by means of light. On the other hand, from Eq. (9) one can see that the virtual polariton mode component E_z neither vanishes outside the slab nor diverges within it. This is because for polaritons the dispersion relation of Eq. (10) is not as strict as the volume plasmon dispersion $\Omega = \Omega_P$ and is satisfied also for $\Omega \neq \Omega_P$. In addition, the volume plasmon is a purely electric oscillation with a strictly null magnetic field, whereas the considered virtual polariton modes are accompanied by a magnetic field. In turn, even though TM polariton modes and volume plasmons occur in the same spectral region and are accidentally connected by the fact that in the limit $L \gg \lambda$ the Lorentz slab is almost equivalent to a bulk medium, conceptually they are very distinct entities. In view of this, we conclude by remarking that volume plasmons cannot be excited by classical light and that the absorption peak observed in experiments [30,32] is due to the excitation of virtual polariton modes, confirming the results given in Refs. [29,31].

IV. CONCLUSIONS

In conclusion, we have investigated both numerically and analytically the properties of the time-domain ENZ regime. Specifically we have considered a dielectric slab whose polarization dynamics has been described through the realistic and ubiquitous Lorentz model, and we have analyzed its interaction with quasimonochromatic and spatially confined pulses with carrier frequencies close to the crossing point of the permittivity real part. The FDTD analysis has shown that the pulse is able to excite a polarization-electromagnetic (polariton) oscillation which is damped and persists for a time generally longer than the effective time required by the pulse for passing through the slab. The underlying nature of this excitation has been elucidated through the analysis of the slab virtual modes that turn out to be located in a portion of the complex frequency plane close to the plasmonic frequency characterizing plasmon and phonon longitudinal volume excitations. Remarkably, due to this spectral property, both the group velocity and the transverse velocity (parallel to the slab) of each virtual mode turn out to be very small and, therefore, the time-domain ENZ regime can be naturally regarded as an alternative platform for discussing and investigating a plethora of slow-light phenomena.

[1] K. L. Tsakmakidis, A. D. Boardman, and O. Hess, Nat. Lett. **450**, 397 (2007).
[2] R. W. Boyd, J. Mod. Opt. **56**, 1908 (2009).
[3] K. H. Kim, A. Husakou, and J. Herrmann, Opt. Express **20**, 25790 (2012).
[4] Y. A. Vlasov, M. O'Boyle, H. F. Hamann, and S. J. McNab, Nature (London) **438**, 65 (2005).
[5] S. F. Mingaleev, A. E. Miroshnichenko, Y. S. Kivshar, and K. Busch, Phys. Rev. E **74**, 046603 (2006).
[6] M. Bajcsy, S. Hofferberth, V. Balic, T. Peyronel, M. Hafezi, A. S. Zibrov, V. Vuletic, and M. D. Lukin, Phys. Rev. Lett. **102**, 203902 (2009).
[7] S. V. Afshar and T. M. Monro, Opt. Express **17**, 2298 (2009).
[8] A. Marini, R. Hartley, A. V. Gorbach, and D. V. Skryabin, Phys. Rev. A **84**, 063839 (2011).
[9] C. Koos, L. Jacome, C. Poulton, J. Leuthold, and W. Freude, Opt. Express **15**, 5976 (2007).
[10] S. Palomba and L. Novotny, Phys. Rev. Lett. **101**, 056802 (2008).
[11] M. Kauranen and A. V. Zayats, Nat. Photonics **6**, 737 (2012).
[12] A. Ciattoni, C. Rizza, and E. Palange, Phys. Rev. A **81**, 043839 (2010).
[13] A. Ciattoni, C. Rizza, and E. Palange, Phys. Rev. A **83**, 043813 (2011).
[14] M. A. Vincenti, D. de Ceglia, A. Ciattoni, and M. Scalora, Phys. Rev. A **84**, 063826 (2011).
[15] A. Ciattoni and E. Spinozzi, Phys. Rev. A **85**, 043806 (2012).
[16] D. A. Powell, A. Alu, B. Edwards, A. Vakil, Y. S. Kivshar, and N. Engheta, Phys. Rev. B **79**, 245135 (2009).
[17] C. Argyropoulos, P.-Y. Chen, G. D. Aguanno, N. Engheta, and A. Alu, Phys. Rev. B **85**, 045129 (2012).
[18] S. Enoch, G. Tayeb, P. Sabouroux, N. Guerin, and P. Vincent, Phys. Rev. Lett. **89**, 213902 (2002).
[19] A. Alu, F. Bilotti, N. Engheta, and L. Vegni, IEEE Trans. Antennas Propag. **54**, 1632 (2006).
[20] A. Alu and N. Engheta, Phys. Rev. E **72**, 016623 (2005).
[21] M. Silveirinha and N. Engheta, Phys. Rev. Lett. **97**, 157403 (2006).
[22] A. Alu, M. G. Silveirinha, A. Salandrino, and N. Engheta, Phys. Rev. B **75**, 155410 (2007).
[23] G. Castaldi, S. Savoia, V. Galdi, A. Alu, and N. Engheta, Phys. Rev. B **86**, 115123 (2012).
[24] A. A. Asatryan, L. C. Botten, M. A. Byrne, V. D. Freilikher, S. A. Gredeskul, I. V. Shadrivov, R. C. McPhedran, and Y. S. Kivshar, Phys. Rev. B **85**, 045122 (2012).
[25] J. Jackson, *Classical Elctrodynamics* (Wiley, New York, 1999).
[26] A. Archambault, M. Besbes, and J.-J. Greffet, Phys. Rev. Lett. **109**, 097405 (2012).
[27] A. Archambault, T. V. Teperik, F. Marquier, and J. J. Greffet, Phys. Rev. B **79**, 195414 (2009).
[28] N. Ashcroft and N. Mermin, *Solid State Physics* (Harcourt College Publishers, Fort Worth, TX, 1976).
[29] L. Henrard, O. Stephan, and C. Colliex, Synth. Met. **103**, 2502 (1999).
[30] K. Höflich, U. Gösele, and S. Christiansen, Phys. Rev. Lett. **103**, 087404 (2009).
[31] L. Henrard, C. Vandenbem, P. Lambin, and A. A. Lucas, Phys. Rev. Lett. **104**, 149701 (2010).
[32] K. Höflich, U. Gösele, and S. Christiansen, Phys. Rev. Lett. **104**, 149702 (2010).
[33] P. Muys, Opt. Lett. **37**, 4928 (2012).
[34] D. W. Berreman, Phys. Rev. **130**, 2193 (1963).
[35] R. Ruppin and R. Englman, Rep. Prog. Phys. **33**, 149 (1970).
[36] S. Vassant, J.-P. Hugonin, F. Marquier, and J.-J. Greffet, Opt. Express **20**, 23971 (2012).
[37] S. Vassant, A. Archambault, F. Marquier, F. Pardo, U. Gennser, A. Cavanna, J. L. Pelouard, and J. J. Greffet, Phys. Rev. Lett. **109**, 237401 (2012).